Comparison of Nonlinear Filters for Quadcopter Wind Estimation

Hao Chen*, Braydon Revard[†], He Bai[‡] and Jamey Jacob[§] *Oklahoma State University, Stillwater, Oklahoma, 74075*

Wind estimation for small unmanned aerial vehicles (sUAVs) can not only improve their navigation and flight performance, but also be used for environmental studies and meteorology. In this paper, we compare a multiplicative extended Kalman filter (MEKF), a translational EKF (TEKF), and an invariant EKF (IEKF) for quadcopter wind estimation. Through Monte Carlo simulations, we demonstrate that the IEKF offers an improvement in transient performance over the MEKF. We also conduct outdoor experiments to validate the effectiveness of the designed filters. The ground truth wind data is collected via a wind velocity sensor mounted at the top of the quadcopter. The experimental results demonstrate that the MEKF and the IEKF outperform the TEKF and the IEKF outperforms MEKF during the transient stage.

I. Nomenclature

a = specific acceleration vector in the body frame

A = cross-sectional area of the quadcopter

 A_k = state transition matrix of estimators

B = earth's magnetic field expressed in the inertial frame

 b_3 = z-axis basis of the quadcopter body frame

 C_D = drag coefficient

D = drag parameter matrix

E = the output error

 f_d = drag force in the body frame f_c = amplitude of the thrust g = standard gravity acceleration

g = gravity acceleration vector in the body frame

 H_k = observation matrix of estimators

K = gain matrix of the Luenberger observer

 k_{Ω} = thrust model coefficient m = mass of the quadcopter

 p_i = the normalized PWM command for each motor

q = unit quaternion of the quadcopter

 R_b = orientation of the quadcopter with respect to the inertial frame

SO(3) = 3-dimensional special orthogonal group SE(3) = 3-dimensional special Euclidean group

U = input vector of the quadcopter

V = the normalized battery voltage of quadcopter SK8
 v = ground velocity of the quadcopter in the body frame

 v_w = wind vector in the inertial frame

 v_r = relative velocity of the quadcopter in the body frame v_{rs} = relative speed of the quadcopter in the body frame

x = inertial position of the quadcopter

^{*}Ph.D. Candidate, Mechanical and Aerospace Engineering, Oklahoma State University.

[†]Research Engineer, Oklahoma Aerospace Institute for Research and Education.

[‡]Associte Professor, Mechanical and Aerospace Engineering, Oklahoma State University.

[§]Williams Chair and Regents Professor & Executive Director, Oklahoma Aerospace Institute for Research and Education, AIAA Associate Fellow.

X = states vector of the quadcopter

 \hat{X} = estimated state vector of the quadcopter y = measurement equation of the quadcopter

z = altitude of the quadcopter

 y_m = measurements of the quadcopter

 ρ = air density

 ω = angular velocity of the quadcopter in the body frame

 Ω_i = angular velocity of each rotor δ = state errors of the MEKF ϕ = roll angle of the quadcopter = pitch angle of the quadcopter

II. Introduction

Wind has a significant impact on small unmanned aerial vehicle (sUAV) flight safety and efficiency, especially for challenging missions such as urban air mobility (UAM) flights and beyond visual line of sight (BVLOS) operations [1]. Accurate wind velocity information can be fed to specifically designed controllers that can compensate for such wind disturbances to maintain safe and robust flight in uncertain environments [2]. The efficiency of flight can also be improved through optimization of path planning based on wind information [3, 4]. In addition, using sUAV to estimate wind can be used in atmospheric, meteorology research [5], and environmental studies [5, 6].

There are several conventional methods for measuring wind velocities, including ground-based systems such as SoDAR, LiDAR, and wind towers. However, those methods are expensive, immovable or hard to move, and only provide wind velocity estimates in a fixed point or a small area [7]. Another way is to use tethered balloons, which is expensive, labor intensive, and hard to operate [8]. Since sUAV is affordable and flexible, it has become a popular platform for wind measurement and estimation. UAVs can be classified into two main categories: fixed-wing UAVs and rotary-wing UAVs. Each category possesses different advantages in the context of wind estimation [9]. A fixed-wing UAV does not hover in place and must fly horizontally to measure wind. As a result, they are mainly utilized for long-range missions. In comparison, a rotary-wing UAV has the capability of estimating wind profiles or temporal variability of the wind at one location.

The current wind measurement or estimation techniques for rotary UAVs can be summarized into the following four approaches: mounting sensors on multi-rotors [8, 10, 11], static mapping method [8, 11–14], machine learning (ML) method [15–17] and model-based method [6, 18–20]. The first method uses rotary UAVs equipped with different types of anemometers to estimate the wind field. However, this approach may reduce flight endurance due to the weight and power requirements of the sensors and the platform. Obtaining the inertial measurement of the wind may be difficult in strong winds since the motion of the quadcopter in this case is not null. In addition, accurate and reliable wind sensors are typically expensive compared to a UAV platform. The static mapping method explores the relation between the wind vector and the UAV's states, such as the tilt angle or power, by using collected data. However, this method has shown effectiveness only in slight wind fields. ML method is a data-driven method that finds the relationship between quadcopter states/measurements and wind velocity. However, ML method may require high-quality training data, and may be specific to the training data of a particular quadcopter and brittle to extend other quadcopters. The model-based method employs models of the quadcopter dynamics, measurements, thrust, drag, and wind to extract the wind information from the quadcopter's motion.

In this paper, we consider the model-based method for wind estimation using a quadcopter. Given a sUAV's dynamic model and measurements, a common way to fuse their information and estimate states and wind velocity is to use the Kalman filter or extended Kalman filter (EKF). For system dynamics which includes attitude kinematics, it is customary to use a unit quaternion q to represent the attitude of the aircraft instead of the rotation matrix or Euler angles. This choice is made because a unit quaternion offers a global parameterization of the body attitude and proves to be well-suited for computational calculations and simulations. But in this scenario, the EKF fails to uphold the geometry of the quaternion space: the conventional linear error and correction terms do not maintain the quaternion's norm. Therefore, we derive a multiplicative EKF (MEKF) [21, 22] for wind estimation. The MEKF respects the geometry of the quaternion space by computing the error equation with the error $q^{-1} * \hat{q}$. Another solution is to separate the translation and orientation part of the system dynamics and design a transnational EKF (TEKF) for wind estimation based only on the transnational dynamics. The attitude information can be obtained from an attitude and heading reference system (AHRS). The third filter for wind estimation is an invariant EKF (IEKF). In recent years, IEKFs have

been investigated for attitude andor pose estimation [23–25]. Reference [24] demonstrates that IEKF shows superior convergence and robustness properties over MEKF since the error model of the IEKF does not depend on the state estimate. Motivated by the fact that symmetry properties of a dynamical system can be leveraged to improve estimator's performance and stability, we design an IEKF for wind estimation in [26].

The contribution of the paper is that we design a MEKF and a TEKF and compare them with the IEKF in [26] for wind estimation using both simulations and experimental data. Simulation results show that the IEKF outperforms the MEKF in the transient performance. Experimental results also verify the superiority of the IEKF. The rest of the paper is organized as follows. In Section III, we introduce the wind estimation problem which includes quadcopter system dynamics, measurements, and thrust and drag models. In Section IV, we introduce the MEKF and the TEKF and review the IEKF. We conduct Monte Carlo (MC) simulations for the MEKF and the IEKF under various wind fields in Section V. Section VI provides outdoor experimental results, comparing wind estimation performance of the MEKF, the TEKF, and the IEKF. Conclusions and future work are presented in Section VII.

III. Problem Formulation

The translational dynamics and the attitude kinematics of a quadcopter subject to a wind disturbance in the north-east-down (NED) frame are given by [27]:

$$\dot{x} = R_b v$$

$$\dot{v} = v \times \omega + R_b^T \mathbf{g} - \frac{1}{m} f_c b_3 + \frac{1}{m} f_d + R_b^T \dot{v}_w$$

$$\dot{R}_b = R_b S(\omega)$$
(1)

where $x \in \mathbb{R}^3$ is the inertial position, $v \in \mathbb{R}^3$ is the ground velocity in the body frame, $v_w \in \mathbb{R}^3$ is the wind vector in the inertial frame, $R_b \in SO(3)$ is the orientation of the quadcopter with respect to the inertial frame and SO(3) is the 3D special orthogonal group, $m \in \mathbb{R}^+$ is the mass of the quadcopter, $\mathbf{g} = [0,0,g]^T \in \mathbb{R}^3$ denotes the gravity acceleration vector in the body frame, $\omega \in \mathbb{R}^3$ is the angular velocity of the quadcopter in the body frame, the function $S(\cdot) : \mathbb{R}^3 \to so(3)$ satisfies $S(a)b = a \times b$ for $a, b \in \mathbb{R}^3$ where so(3) denotes lie algebra of the SO(3). $f_c \in \mathbb{R}^+$ is the amplitude of the thrust control input and $f_cb_3 \in \mathbb{R}^3$ in which $b_3 = [0,0,1]^T$ denotes the thrust vector in body frame. We consider a nominal thrust model in the simulation section and find that a polynomial thrust model is sufficient for horizontal wind estimation in the experiment section. More complicated thrust models can be found in [28]. $f_d \in \mathbb{R}^3$ denotes the drag force. Drag is a force that acts opposite to the relative motion of any object moving with respect to a surrounding fluid. The drag force is an aerodynamic force that opposes an aircraft's motion through the air. Normally the drag equation [7, 15, 27] is given by

$$f_d = \frac{1}{2}\rho C_D A v_{rs}^2 \tag{2}$$

where ρ is the air density, v_{rs} is the relative speed of the aircraft to the air, A is the cross-sectional area, and C_D is the drag coefficient which is a dimensionless number. In this paper, we adapt the above one-dimensional drag force equation to a three-dimensional drag vector equation

$$f_d = -\frac{1}{2}\rho D|v_r|v_r, \quad D = \begin{pmatrix} D_x & 0 & 0\\ 0 & D_y & 0\\ 0 & 0 & D_z \end{pmatrix},\tag{3}$$

where $v_r \in \mathbb{R}^3$ is the relative velocity vector given by $v_r = v - R_b^T v_w$, and $D \in \mathbb{R}^{3 \times 3}$ is a drag parameter matrix, which can be regarded as the combined representation of the drag coefficient and the cross-sectional area.

We model the wind dynamics as $\dot{v}_w = 0$ which models a constant mean wind. In the filter implementation, we add process noise to the v_w dynamics to mitigate the effect of the turbulent component in the wind. Combining the wind model, we rewrite the system dynamics in (1) in terms of x, v_r , R_b , and v_w as

$$\dot{x} = R_b v_r + v_w$$

$$\dot{v}_r = v_r \times \omega + R_b^T \mathbf{g} - \frac{1}{m} f_c b_3 + \frac{1}{m} f_d$$

$$\dot{R}_b = R_b S(\omega)$$

$$\dot{v}_w = 0.$$
(4)

We assume that the quadcopter is equipped with a GPS, a 3-axis accelerometer and gyroscope, and a magnetometer. The measured angular velocity from the gyroscope is used in the system dynamics as one of the inputs. The measurement equation $y = (y_x^T, y_a^T, y_b^T)^T$ is given by

$$y = \begin{pmatrix} y_x \\ y_a \\ y_b \end{pmatrix} = \begin{pmatrix} x \\ a \\ R_b^T B \end{pmatrix}$$
 (5)

where $B \in \mathbb{R}^3$ is the earth's magnetic field expressed in the inertial frame and $a \in \mathbb{R}^3$ is the specific acceleration vector in the body frame given by

$$a = \frac{1}{m} \left(-f_c b_3 + f_d \right). \tag{6}$$

Biases in the angular velocity and acceleration measurements are assumed to be calibrated out.

IV. Wind Estimation Filters

A. MEKF

In this section, we introduce a multiplicative extended Kalman filter (MEKF) [21] for wind estimation. Let $q \in \mathbb{R}^4$ be the unit quaternion representing R_b and * denotes the quaternion multiplication. Then the system dynamics (4) becomes

$$\dot{x} = q * v_r * q^{-1} + v_w$$

$$\dot{v}_r = v_r \times \omega + q^{-1} * \mathbf{g} * q - \frac{1}{m} f_c b_3 + \frac{1}{m} f_d$$

$$\dot{q} = \frac{1}{2} q * \omega$$

$$\dot{v}_w = 0.$$
(7)

In a quaternion multiplication, any vector in \mathbb{R}^3 is augmented to a quaternion with 0 being the scalar part. Similarly, the measurement equation (5) where the rotation is represented by the unit quaternion is rewritten as

$$y = \begin{pmatrix} y_x \\ y_a \\ y_b \end{pmatrix} = \begin{pmatrix} x \\ a \\ q^{-1} * B * q \end{pmatrix}. \tag{8}$$

We define $\hat{X} = (\hat{x}^T, \hat{v}_r^T, \hat{q}^T, \hat{v}_w^T)^T$ as the estimated states vector and $U = (\omega^T, f_c)^T$ as the inputs vector. The MEKF takes the form of

$$\dot{\hat{x}} = \hat{q} * \hat{v}_r * \hat{q}^{-1} + \hat{v}_w + K_x E
\dot{\hat{v}}_r = \hat{v}_r \times \omega + \hat{q}^{-1} * \mathbf{g} * \hat{q} - \frac{1}{m} f_c b_3 + \frac{1}{m} \hat{f}_d + K_{v_r} E
\dot{\hat{q}} = \frac{1}{2} \hat{q} * \omega + \hat{q} * (K_q E)
\dot{\hat{v}}_w = 0 + K_{v_w} E$$
(9)

where $\hat{f}_d = -\frac{1}{2}\rho D|\hat{v}_r|\hat{v}_r$ and $K = (K_x^T, K_{v_r}^T, K_q^T, K_{v_w}^T)^T$ is the gain matrix.

We consider the state error

$$\begin{pmatrix} \delta_{x} \\ \delta_{v_{r}} \\ \delta_{q} \\ \delta_{v_{w}} \end{pmatrix} = \begin{pmatrix} \hat{x} - x \\ \hat{v}_{r} - v_{r} \\ q^{-1} * \hat{q} \\ \hat{v}_{w} - v_{w} \end{pmatrix}, \tag{10}$$

whose dynamics is given by

$$\begin{aligned}
\dot{\delta_{x}} &= \dot{\hat{x}} - \dot{x} \\
&= \hat{q} * \hat{v}_{r} * \hat{q}^{-1} - q * v_{r} * q^{-1} + \hat{v}_{w} - v_{w} + K_{x}E \\
&= \hat{q} * \hat{v}_{r} * \hat{q}^{-1} - \hat{q} * \delta_{q}^{-1} * (\hat{v}_{r} - \delta_{v_{r}}) * \delta_{q} * \hat{q}^{-1} + \delta_{v_{w}} + K_{x}E \\
\dot{\delta_{v_{r}}} &= \dot{\hat{v}_{r}} - \dot{v}_{r} \\
&= (\hat{v}_{r} - v_{r}) \times \omega + (\hat{q}^{-1} * \mathbf{g} * \hat{q} - q^{-1} * \mathbf{g} * q) + \frac{1}{m} \left(\hat{f}_{d} - f_{d} \right) + K_{v_{r}}E \\
&= \delta_{v_{r}} \times \omega + (\hat{q}^{-1} * \mathbf{g} * \hat{q} - \delta_{q} * \hat{q}^{-1} * \mathbf{g} * \hat{q} * \delta_{q}^{-1}) + \frac{1}{m} \delta_{f_{d}} + K_{v_{r}}E \\
\dot{\delta_{q}} &= \dot{q}^{-1} * \hat{q} + q^{-1} * \dot{q} \\
&= (-q^{-1} * \dot{q} * q^{-1}) * \hat{q} + q^{-1} * (\frac{1}{2} \hat{q} * \omega + \hat{q} * (K_{q}E)) \\
&= \delta_{q} \times \omega + \delta_{q} * (K_{q}E) \\
\dot{\delta_{v_{w}}} &= \dot{v}_{w} - \dot{v}_{w} = K_{v_{w}}E,
\end{aligned} \tag{11}$$

where $\delta_{f_d} = \hat{f_d} - f_d = \left(-\frac{1}{2}\rho D\left(|\hat{v}_r|\hat{v}_r - |\hat{v}_r - \delta_{v_r}|(\hat{v}_r - \delta_{v_r})\right)\right)$. The output error is

$$E = \begin{pmatrix} \hat{x} - x \\ \hat{a} - a \\ \hat{q}^{-1} * B * \hat{q} - q^{-1} * B * q \end{pmatrix} = \begin{pmatrix} \delta_{x} \\ \frac{1}{m} \delta_{f_{d}} \\ \hat{q}^{-1} * B * \hat{q} - \delta_{q} * \hat{q}^{-1} * B * \hat{q} * \delta_{q}^{-1} \end{pmatrix}.$$
(12)

Then we linearize the error dynamics and the output error around $(\delta_x, \delta_{v_r}, \delta_q, \delta_{v_w}) = [0, 0, 1, 0]$ to obtain $A_k = \frac{\partial \dot{\delta}}{\partial \delta}$ and $H_k = \frac{\partial E}{\partial \delta}$ needed for implementing the MEKF:

$$A_{k} = \begin{pmatrix} 0_{33} & R(\hat{q}) & \frac{\partial (-R(\hat{q})R^{T}(\delta_{q})(\hat{v}_{r} - \delta_{v_{r}}))}{\partial \delta_{q}} & I_{33} \\ 0_{33} & -S(\omega) + \frac{1}{m} \frac{\partial \delta_{f_{d}}}{\partial \delta_{v_{r}}} & \frac{\partial (-R(\delta_{q})R^{T}(\hat{q})\mathbf{g})}{\partial \delta_{q}} & 0_{33} \\ 0_{33} & 0_{33} & (0_{31} S(-\omega)) & 0_{33} \\ 0_{33} & 0_{33} & 0_{34} & 0_{33} \end{pmatrix},$$
(13)

$$H_{k} = \begin{pmatrix} I_{33} & 0_{33} & 0_{34} & 0_{33} \\ 0_{33} & \frac{1}{m} \frac{\partial \delta_{f_{d}}}{\partial \delta_{v_{r}}} & 0_{34} & 0_{33} \\ 0_{33} & 0_{33} & \frac{\partial (-R(\delta_{q})R^{T}(\hat{q})B)}{\partial \delta_{c}} & 0_{33} \end{pmatrix}$$
(14)

where 0_{mn} is the m by n zero matrix, I_{33} is the 3 by 3 identity matrix, and $R(\hat{q})$ and $R(\delta_q)$ denote the rotation matrices represented by the estimated quaternion \hat{q} and the quaternion error δ_q , respectively. The MEKF algorithm is given in Algorithm 1 below.

B. TEKF

Motivated by [29], we also design and implement a translational EKF (TEKF) for wind estimation. Such TEKF only considers the translational dynamics of the system

$$\dot{x} = q * v_r * q^{-1} + v_w$$

$$\dot{v}_r = v_r \times \omega + q^{-1} * \mathbf{g} * q - \frac{1}{m} f_c b_3 + \frac{1}{m} f_d$$

$$\dot{v}_w = 0$$
(15)

and the measurement equation is y = x. The TEKF is based on the ease of design, tuning, and the better computational efficiency compared to the full-state MEKF. The attitude information R_b can be obtained from an attitude and heading

Algorithm 1: MEKF

```
1 Initialize X_0, P_0

2 for k=1 to n do

3 Prediction: in between measurements (t \in [t_{k-1}, t_k])

4 Propagate \dot{\hat{X}} = f(\hat{X}, U) according to (9) with K_k = 0 to get \hat{X}_k^-

5 Compute A_k from (13)

6 Propagate \dot{P} = A_k P + P A_k^T + Q_k to get P_k^-

7 Correction: at the k^{th} sensor measurement (t = t_k)

8 Compute H_k from (14)

9 K_k = P_k^- H_k^T (H_k P_k^- H_k^T + R_k)^{-1}

10 \hat{X}_k^+ = \hat{X}_k^- + K_k (y_{m,k} - h(\hat{X}_k^-, U))

11 P_k^+ = (I - K_k H_k) P_k^-

12 end
```

reference system (AHRS) or a built-in filter from an autopilot (e.g., the Ardupilot). The TEKF is cascaded to the attitude filter. The corresponding TEKF takes the form of

$$\dot{\hat{x}} = \hat{q} * \hat{v}_r * \hat{q}^{-1} + \hat{v}_w + K_x E
\dot{\hat{v}}_r = \hat{v}_r \times \omega + \hat{q}^{-1} * \mathbf{g} * \hat{q} - \frac{1}{m} f_c b_3 + \frac{1}{m} \hat{f}_d + K_{v_r} E
\dot{\hat{v}}_w = 0 + K_{v_w} E.$$
(16)

We define $\hat{X} = (\hat{x}^T, \hat{v}_r^T, \hat{v}_w^T)^T$ as the estimated states vector and $U = (q^T, \omega^T, f_c)^T$ as the inputs vector for the TEKF. Consider the state error

$$\begin{pmatrix} \delta_{x} \\ \delta_{v_{r}} \\ \delta_{v_{w}} \end{pmatrix} = \begin{pmatrix} \hat{x} - x \\ \hat{v}_{r} - v_{r} \\ \hat{v}_{w} - v_{w} \end{pmatrix}, \tag{17}$$

whose error dynamics is as follows

$$\dot{\delta_{x}} = \hat{q} * \delta_{v_{r}} * \hat{q}^{-1} + \delta_{v_{w}} + K_{x}E$$

$$\dot{\delta_{v_{r}}} = \delta_{v_{r}} \times \omega + \frac{1}{m} \delta_{f_{d}} + K_{v_{r}}E$$

$$\dot{\delta_{v_{w}}} = K_{v_{w}}E$$
(18)

where $\delta_{f_d} = \left(-\frac{1}{2}\rho D\left(|\hat{v}_r|\hat{v}_r - |\hat{v}_r - \delta_{v_r}|(\hat{v}_r - \delta_{v_r})\right)\right)$ and the output error is $E = \hat{x} - x = \delta_x$. Then we linearize the error dynamics and the output error around $(\delta_x, \delta_{v_r}, \delta_{v_w}) = [0, 0, 0]$ to obtain $A_k = \frac{\partial \dot{\delta}}{\partial \delta}$ and $H_k = \frac{\partial E}{\partial \delta}$ as

$$A_{k} = \begin{pmatrix} 0_{33} & R(\hat{q}) & I_{33} \\ 0_{33} & -S(\omega) + \frac{1}{m} \frac{\partial \delta_{f_{d}}}{\partial \delta_{v_{r}}} & 0_{33} \\ 0_{33} & 0_{33} & 0_{33} \end{pmatrix},$$
(19)

$$H_k = \begin{pmatrix} I_{33} & 0_{33} & 0_{33} \end{pmatrix}. \tag{20}$$

Similar to MEKF, the A_k and H_k will be used for propagation and correction of the TEKF.

C. IEKF

In [26], we design an invariant EKF (IEKF) for wind estimation. The IEKF leverages symmetries in the system dynamics associated with the special Euclidean group G = SE(3). We construct transformations on states, inputs and the measurement equation such that the system dynamics is invariant and the measurement equation is equivariant.

The IEKF design follows the method outlined in [23], and [26] provides the detailed derivation. Note that the IEKF is designed based on an invariant state error rather than the state error of the MEKF. We employ the nominal thrust model in Section V and a polynomial thrust model as in Section VI. The thrust is treated as one of the inputs to the system. For more advanced thrust models, the transformations may need to be specially designed for an IEKF and we refer to [28] for details.

V. Simulations

In this section, we conduct simulations and compare the estimation performance of the quadcopter states and the wind between the MEKF and the IEKF for different wind fields. The first one is a constant wind equal to $(3, 2, 0)^T$ m/s. The second and third wind fields are generated from a large eddy simulation (LES) [30] capturing the low-altitude turbulence effect. Both LES wind fields have a mean wind of approximately $(3, 2, 0)^T$ m/s at different altitudes. The wind field at 50 meters is much more turbulent than at 8 meters. We construct a quadcopter simulink model which consists of the quadcopter dynamics, position controllers, attitude controllers, a motor model, a rotor model, a wind model, and a sensor model. The sensor model simulates that the quadcopter is equipped with a GPS, an accelerometer, a gyroscope, and a magnetometer.

We conduct Monte Carlo (MC) simulations of 50 runs. For each MC run, the quadcopter flies from a random starting point around the origin in the inertial frame to a goal point and then hovers at that point. The thrust model is the nominal thrust model $f_c = k_{\Omega} \sum_{i=1}^{4} \Omega_i^2$ where k_{Ω} is the thrust model coefficient and Ω_i is the angular velocity of the rotor. We test the three wind fields for the comparison of the MEKF and the IEKF. All the simulation results show that the IEKF has better transient estimation performance compared to the MEKF. For example, Fig. 1 is the wind estimation results from one run of the MC simulations. We observe that the estimated wind of the IEKF has a much smaller error at the beginning and converges more quickly compared to the wind estimates of the MEKF. At the steady state, the wind estimation of both filters shows similar performance. Meanwhile, from the constant wind test to the LES wind (8m) test and the LES wind (50m) test, the superiority of the IEKF gradually decreases. This can be explained by that the LES wind, especially at 50 meters, contains more turbulence, which degrades the symmetry of the system. In Fig. 2, we show the root mean square error (RMSE) of the position estimates in the north direction, the relative velocity estimates in the x direction, the roll angle estimates, and the wind velocity estimates in the north direction between the MEKF and the IEKF for the first 30 seconds. The RMSE used in MC simulations is defined as

$$RMSE_{i}(k) = \sqrt{\frac{\sum_{j=1}^{n} (X_{i,j}(k) - \hat{X}_{i,j}(k))^{2}}{n}}$$
(21)

where $X_{i,j}(k)$ represent the *i*th element of states at time k in the *j*th run and $\hat{X}_{i,j}(k)$ represents the estimates of $X_{i,j}(k)$. From the simulation results, we observe that the IEKF has better transient performance compared to the MEKF. In this section, we compare only the MEKF and the IEKF as they both estimate the full state vector, including the translational states and the attitude. The performance of the TEKF depends on the attitude filter performance. We choose to compare the performance of the TEKF using only experimental data as the attitude filter is readily available from the onboard autopilot.

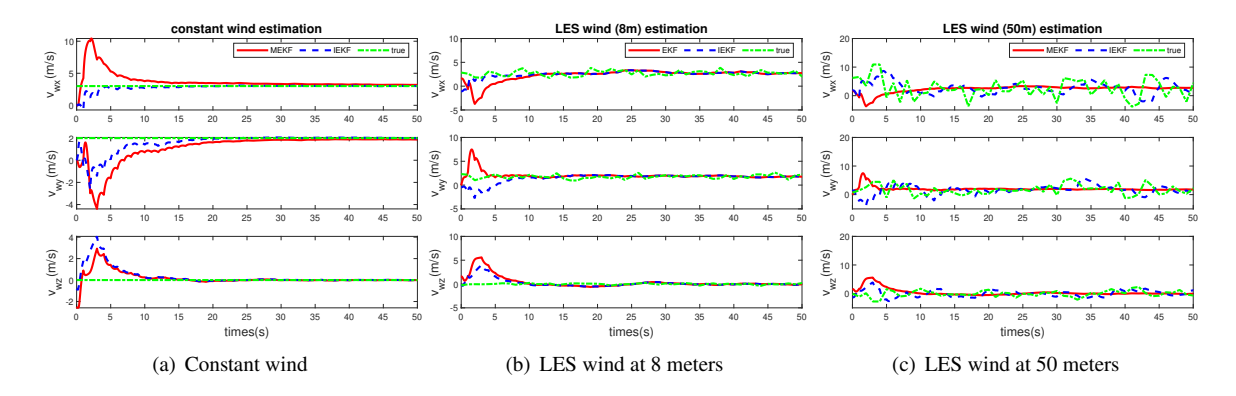
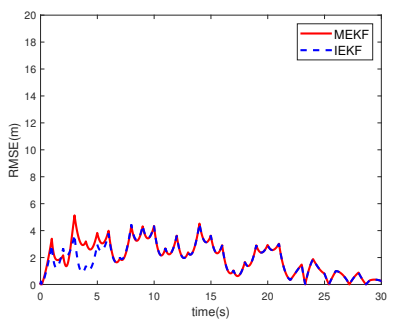
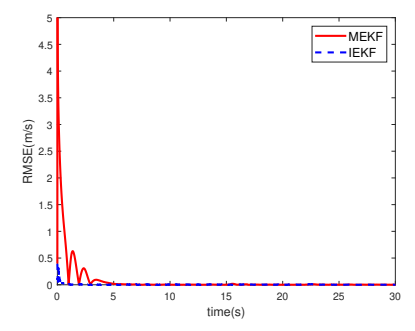
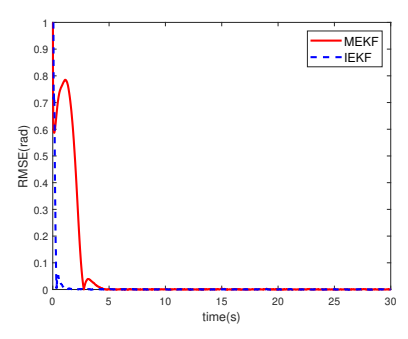


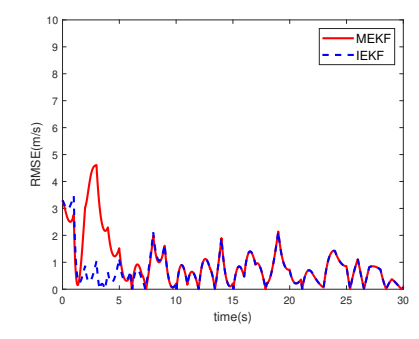
Fig. 1 The MEKF and the IEKF wind estimation performance under various wind fields.





(a) RMSE of the *x*-component of position estimates in the(b) RMSE of the *x*-component of relative velocity estimates in the body frame





(c) RMSE of roll angle estimates (d) RMSE of the *x*-component of wind velocity estimates in the inertial frame

Fig. 2 RMSE of MEKF and IEKF estimates for LES wind at 8 meters.

VI. Experiments

A. Experimental Setup

We design and develop a large size quadcopter SK8 as shown in Fig. 3, which is used to perform hover tests and collect data in an outdoor environment. SK8 is a self-built quadcopter from Oklahoma State University Unmanned Systems Research Institute (USRI). There is a TriSonica Mini anemometer mounted on the top of a gimbal to collect measured wind data for comparison.

We have conducted three separate outdoor experiments and seven datasets of hover tests are collected. For each experiment, the experimental locations (Oklahoma State University (OSU) Unmanned Aircraft Flight Station (UAFS) and OSU campus) and dates (Oct. 17, 2022, Dec. 1, 2022 and May 31, 2023) are carefully selected based on the safety and suitability of the wind field. We use a logging tool provided by Pixhawk4 to log the GPS data at 5Hz, IMU (including gyroscope, accelerometer and magnetometer) data at 200Hz, in-built EKF estimated states at 10Hz and PWM data at 10Hz separately. Also, we use an Arduino board to log the Anemometer data at 5Hz.

B. Calibration Methodology

To estimate the wind, a thrust model is required. For the large scale quadcopter SK8 equipped with large-sized blades, building a thrust stand and conducting the wind tunnel test is challenging and expensive. Instead, we use a polynomial thrust model to obtain the thrust from a calibration dataset. We first define z as the altitude of the quadcopter and $R_{b,3}$ as the third row of the rotation matrix R_b . Consider the translational dynamics of the quadcopter in the z direction in the inertial frame

$$\ddot{z} = \frac{1}{m} R_{b,3} f_c b_3 - \mathbf{g} - \frac{1}{m} R_{b,3} f_d. \tag{22}$$





Fig. 3 SK8 quadcopter.

Fig. 4 SK8 in a hover experiment.

We make the assumption that the drag force in z direction of the body frame is small compared to the thrust. Thus we ignore the drag force term in (22) to obtain

$$\ddot{z} \approx \frac{f_c}{m} \cos \theta \cos \phi - g \tag{23}$$

where ϕ and θ are roll and pitch angles of the quadcopter respectively. Assume that there is little vertical motion when the quadcopter is hovering. We obtain the simple projection thrust via

$$f_c = \frac{mg}{\cos\theta\cos\phi}. (24)$$

For the polynomial thrust model, we use the thrust data obtained from (24) based on the calibration dataset and fit a polynomial thrust model [31]

$$f_c = f(V, p_i) = a_1 - a_2 \sum_{i=1}^4 p_i - a_3 V + a_4 \sum_{i=1}^4 p_i^2 + a_5 \sum_{i=1}^4 p_i V,$$

where *V* is the normalized battery voltage, p_i is the normalized PWM command for motor i (i = 1, 2, 3, 4), and $[a_1 \ a_2 \ a_3 \ a_4 \ a_5] = [78.2270 \ 1.0525 \ 0.6386 \ 0.8445 \ 1.1095]$.

Using the calibration test data, a linear regression with the basis function below is used to find the drag parameter matrix

$$f_d = D\Phi(v_r) \tag{25}$$

where $\Phi(v_r) = -\frac{1}{2}\rho|v_r|v_r$ and the drag force vector in the body frame is obtained as

$$f_d = R_b^T (R_b \dot{v}_r - m\mathbf{g} - R_b (f_c b_3)). \tag{26}$$

Through the linear regression, the drag parameter matrix is identified as $D = diag([0.36\ 0.28\ 0.35])$ for the quadratic drag model. The IMU biases are calibrated by the Mission Planner before every tests.

C. Experimental Results

Table 1 Horizontal wind speed estimation.

estimator	error metric	test1	test2	test3	test4	test5	test6
TEKF	RMSE	1.3910	1.3905	2.3445	2.6582	1.2406	1.4602
MEKF	RMSE	1.2649	1.0237	1.4799	1.2073	1.1963	1.5602
IEKF	RMSE	1.1201	0.9908	1.3953	1.2296	0.9774	1.5127

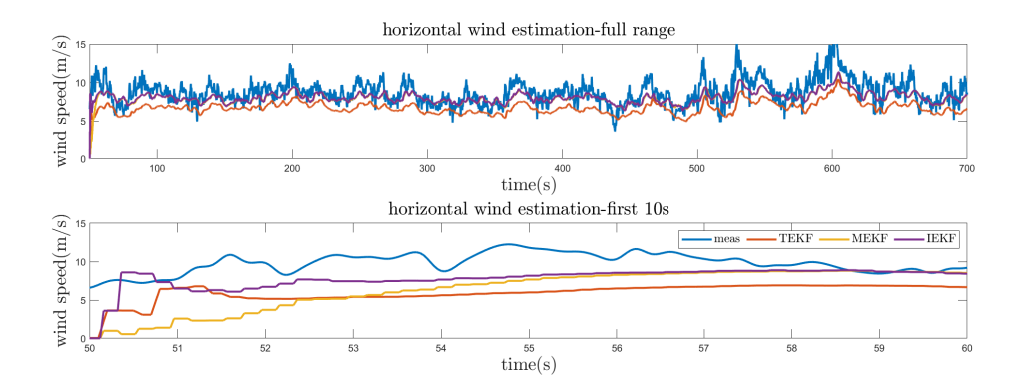


Fig. 5 Horizontal wind speed estimation of various estimators based on test3. Note that the 'meas' in the legend denotes the measured wind speed from the anemometer.

from test3. The IEKF and the MEKF perform similarly and they are both better than the TEKF. The wind estimation performance of the IEKF and the MEKF shows difference mainly in the transient stage.

Table 2 and Table 3 show wind estimation RMSE of the three estimators at the full range and for the first 30 seconds of each dataset, respectively. From Table 2, we see that the RMSE of the TEKF is significantly greater than that of MEKF/IEKF for all the tests, which proves that the TEKF is not an optimal estimator compared to the MEKF/IEKF. For the IEKF, the RMSE is smaller than that of the MEKF, which is explained by the superiority of the IEKF's transient stability. Since Table 3 shows the first 30 seconds of estimators, we also observe such trend more clearly: the IEKF is more stable at the transient stage compared to the MEKF. From Fig. 6, we observe the above properties intuitively: (1) The RMSE of the TEKF is greater than the MEKF/IEKF; (2) The MEKF has a larger transient RMSE compared to the IEKF but behaves similarly to the IEKF in the steady state.

VII. Conclusion

We investigate the model-based wind estimation method for a quadcopter and focus on comparison of three estimators: TEKF, MEKF and IEKF. We conduct simulations and demonstrate that the IEKF outperforms the MEKF at the transient stage. We also perform outdoor experiments and collect relevant data to compare the filters. Our results from the experimental data indicate that the MEKF and the IEKF have better overall perform when compared to the TEKF. In addition, the IEKF shows less transient error and converges faster when compared to the MEKF. Future work includes estimating a spatial-temporal wind field and fusing wind information from multiple quadcopters.

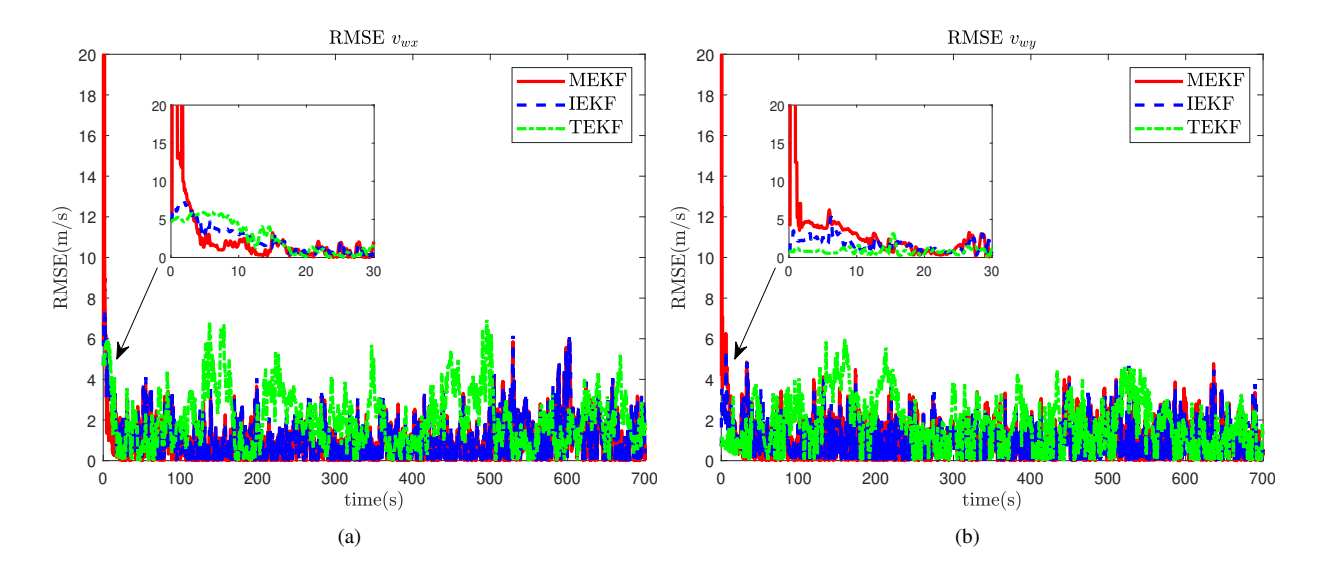


Fig. 6 RMSE comparison of the TEKF/MEKF/IEKF for test3. (a): RMSE v_{w_x} . (b): RMSE v_{w_y} .

Table 2 Wind estimation RMSE (full range) of the estimators with the polynomial thrust model and the quadratic drag model.

estimator type	wind vector	test1	test2	test3	test4	test5	test6
TEKF	v_{wx}	1.3022	1.7990	2.1862	2.3399	1.6611	2.6559
TEKF	v_{wy}	2.2238	2.2079	1.6496	1.8295	1.6789	2.3767
MEKF	v_{wx}	1.2356	1.1113	1.1408	1.6020	1.4033	1.6052
MEKF	v_{wy}	2.0424	1.8063	1.2156	1.5077	1.0682	1.5115
IEKF	v_{wx}	0.9032	0.8841	1.0796	1.2158	1.2044	1.4727
IEKF	v_{wy}	1.5912	1.3280	1.1290	1.5789	0.9503	1.3987

Table 3 Wind estimation RMSE (first 30 seconds) of the estimators with the polynomial thrust model and the quadratic drag model.

estimator type	wind vector	test1	test2	test3	test4	test5	test6
TEKF	v_{wx}	2.1014	1.3174	2.4701	2.6738	1.0027	1.1061
TEKF	v_{wy}	1.1762	0.5855	1.2491	1.9580	1.0982	1.4921
MEKF	v_{wx}	2.6493	1.2992	2.3885	4.3157	3.4127	2.8852
MEKF	v_{wy}	3.5733	3.1335	1.6772	3.8600	2.3752	2.2005
IEKF	v_{wx}	2.2375	1.2773	1.8341	2.4171	1.5852	1.7356
IEKF	v_{wy}	2.3161	2.5511	1.0920	4.3197	1.4576	1.4606

Acknowledgment

The work is supported by the National Science Foundation (NSF) under Grant No. 1925147.

References

^[1] Tian, P., Chao, H., Rhudy, M., Gross, J., and Wu, H., "Wind sensing and estimation using small fixed-wing unmanned aerial vehicles: A survey," *Journal of Aerospace Information Systems*, Vol. 18, No. 3, 2021, pp. 132–143.

- [2] Tabassum, A., Vuppala, R. K., Bai, H., and Kara, K., "Variance reduction of quadcopter trajectory tracking in turbulent wind," *IFAC-PapersOnLine*, Vol. 54, No. 20, 2021, pp. 102–107.
- [3] Thanellas, G. A., Moulianitis, V. C., and Aspragathos, N. A., "A spatially wind aware quadcopter (UAV) path planning approach," *IFAC-PapersOnLine*, Vol. 52, No. 8, 2019, pp. 283–288.
- [4] Patrikar, J., Dugar, V., Arcot, V., and Scherer, S., "Real-time motion planning of curvature continuous trajectories for urban UAV operations in wind," 2020 International Conference on Unmanned Aircraft Systems (ICUAS), IEEE, 2020, pp. 854–861.
- [5] González-Rocha, J., Bilyeu, L., Ross, S. D., Foroutan, H., Jacquemin, S. J., Ault, A. P., and Schmale, D. G., "Sensing atmospheric flows in aquatic environments using a multirotor small uncrewed aircraft system (sUAS)," *Environmental Science: Atmospheres*, 2023.
- [6] Wang, J.-Y., Luo, B., Zeng, M., and Meng, Q.-H., "A wind estimation method with an unmanned rotorcraft for environmental monitoring tasks," *Sensors*, Vol. 18, No. 12, 2018, p. 4504.
- [7] McConville, A., Richardson, T. S., and Moradi, P., "Comparison of Multirotor Wind Estimation Techniques Through Conventional On-board Sensors," *AIAA SCITECH 2022 Forum*, 2022, p. 0411.
- [8] Palomaki, R. T., Rose, N. T., van den Bossche, M., Sherman, T. J., and De Wekker, S. F., "Wind estimation in the lower atmosphere using multirotor aircraft," *Journal of Atmospheric and Oceanic Technology*, Vol. 34, No. 5, 2017, pp. 1183–1191.
- [9] Prudden, S., Fisher, A., Marino, M., Mohamed, A., Watkins, S., and Wild, G., "Measuring wind with small unmanned aircraft systems," *Journal of Wind Engineering and Industrial Aerodynamics*, Vol. 176, 2018, pp. 197–210.
- [10] De Boisblanc, I., Dodbele, N., Kussmann, L., Mukherji, R., Chestnut, D., Phelps, S., Lewin, G. C., and de Wekker, S., "Designing a hexacopter for the collection of atmospheric flow data," 2014 Systems and Information Engineering Design Symposium (SIEDS), IEEE, 2014, pp. 147–152.
- [11] Wolf, C. A., Hardis, R. P., Woodrum, S. D., Galan, R. S., Wichelt, H. S., Metzger, M. C., Bezzo, N., Lewin, G. C., and de Wekker, S. F., "Wind data collection techniques on a multi-rotor platform," 2017 Systems and Information Engineering Design Symposium (SIEDS), IEEE, 2017, pp. 32–37.
- [12] Neumann, P. P., and Bartholmai, M., "Real-time wind estimation on a micro unmanned aerial vehicle using its inertial measurement unit," *Sensors and Actuators A: Physical*, Vol. 235, 2015, pp. 300–310.
- [13] Brosy, C., Krampf, K., Zeeman, M., Wolf, B., Junkermann, W., Schäfer, K., Emeis, S., and Kunstmann, H., "Simultaneous multicopter-based air sampling and sensing of meteorological variables," *Atmospheric Measurement Techniques*, Vol. 10, No. 8, 2017, pp. 2773–2784.
- [14] Marino, M., Fisher, A., Clothier, R., Watkins, S., Prudden, S., and Leung, C. S., "An evaluation of multi-rotor unmanned aircraft as flying wind sensors," *International Journal of Micro Air Vehicles*, Vol. 7, No. 3, 2015, pp. 285–299.
- [15] Allison, S., Bai, H., and Jayaraman, B., "Wind estimation using quadcopter motion: A machine learning approach," *Aerospace Science and Technology*, Vol. 98, 2020, p. 105699.
- [16] Crowe, D., Pamula, R., Cheung, H. Y., and De Wekker, S. F., "Two supervised machine learning approaches for wind velocity estimation using multi-rotor copter attitude measurements," *Sensors*, Vol. 20, No. 19, 2020, p. 5638.
- [17] Zimmerman, S., Yeremi, M., Nagamune, R., and Rogak, S., "Wind estimation by multirotor dynamic state measurement and machine learning models," *Measurement*, Vol. 198, 2022, p. 111331.
- [18] González-Rocha, J., Woolsey, C. A., Sultan, C., and De Wekker, S. F., "Model-based wind profiling in the lower atmosphere with multirotor UAS," AIAA Scitech 2019 Forum, 2019, p. 1598.
- [19] González-Rocha, J., De Wekker, S. F., Ross, S. D., and Woolsey, C. A., "Wind profiling in the lower atmosphere from wind-induced perturbations to multirotor UAS," *Sensors*, Vol. 20, No. 5, 2020, p. 1341.
- [20] Simma, M., Mjøen, H., and Boström, T., "Measuring wind speed using the internal stabilization system of a quadrotor drone," *Drones*, Vol. 4, No. 2, 2020, p. 23.
- [21] Martin, P., and Salaün, E., "Generalized multiplicative extended kalman filter for aided attitude and heading reference system," *AIAA Guidance, Navigation, and Control Conference*, 2010, p. 8300.

- [22] Chang, L., "Multiplicative extended Kalman filter ignoring initial conditions for attitude estimation using vector observations," *The Journal of Navigation*, Vol. 76, No. 1, 2023, pp. 62–76.
- [23] Bonnabel, S., Martin, P., and Rouchon, P., "Symmetry-preserving observers," *IEEE Transactions on Automatic Control*, Vol. 53, No. 11, 2008, pp. 2514–2526.
- [24] Barrau, A., and Bonnabel, S., "Intrinsic filtering on Lie groups with applications to attitude estimation," *IEEE Transactions on Automatic Control*, Vol. 60, No. 2, 2014, pp. 436–449.
- [25] Barrau, A., and Bonnabel, S., "The invariant extended Kalman filter as a stable observer," *IEEE Transactions on Automatic Control*, Vol. 62, No. 4, 2016, pp. 1797–1812.
- [26] Chen, H., Bai, H., and Taylor, C. N., "Invariant-EKF design for quadcopter wind estimation," 2022 American Control Conference (ACC), IEEE, 2022, pp. 1236–1241.
- [27] González-Rocha, J., Woolsey, C. A., Sultan, C., and De Wekker, S. F., "Sensing wind from quadrotor motion," *Journal of Guidance, Control, and Dynamics*, Vol. 42, No. 4, 2019, pp. 836–852.
- [28] Chen, H., and Bai, H., "Incorporating thrust models for quadcopter wind estimation," *IFAC-PapersOnLine*, Vol. 55, No. 37, 2022, pp. 19–24.
- [29] Kingston, D., and Beard, R., "Real-time attitude and position estimation for small UAVs using low-cost sensors," *AIAA 3rd" Unmanned Unlimited" Technical Conference, Workshop and Exhibit*, 2004, p. 6488.
- [30] Vuppala, R. K. S. S., and Kara, K., "Large-Eddy Simulation of Atmospheric Boundary-Layer Gusts for Small Unmanned Air Systems," *Bulletin of the American Physical Society*, 2020.
- [31] Shi, G., Hönig, W., Shi, X., Yue, Y., and Chung, S.-J., "Neural-swarm2: Planning and control of heterogeneous multirotor swarms using learned interactions," *IEEE Transactions on Robotics*, Vol. 38, No. 2, 2021, pp. 1063–1079.